

Version 3.0 as of March 15, 2011

Contact persons: Marc Besançon, Frédéric Déliot, Cécile Deterre

Alexander Grohsjean, Yvonne Peters, Elizaveta Shabalina, Slava Sharyy

To be submitted to PLB

Comment to d0-run2eb-010@fnal.gov by Monday, 21nd of March, 5pm for preliminary

Comment to d0-run2eb-010@fnal.gov by Wednesday, 23nd of March, 5pm for publication

DØ INTERNAL DOCUMENT – NOT FOR PUBLIC DISTRIBUTION

author list dated 17 February 2011

Measurement of the $t\bar{t}$ production cross section using dilepton events in $p\bar{p}$ collisions

V.M. Abazov,³⁵ B. Abbott,⁷³ B.S. Acharya,²⁹ M. Adams,⁴⁹ T. Adams,⁴⁷ G.D. Alexeev,³⁵ G. Alkhazov,³⁹
A. Alton^{a,61} G. Alverson,⁶⁰ G.A. Alves,² L.S. Ancu,³⁴ M. Aoki,⁴⁸ M. Arov,⁵⁸ A. Askew,⁴⁷ B. Åsman,⁴¹
O. Atramentov,⁶⁵ C. Avila,⁸ J. BackusMayes,⁸⁰ F. Badaud,¹³ L. Bagby,⁴⁸ B. Baldin,⁴⁸ D.V. Bandurin,⁴⁷
S. Banerjee,²⁹ E. Barberis,⁶⁰ P. Baringer,⁵⁶ J. Barreto,³ J.F. Bartlett,⁴⁸ U. Bassler,¹⁸ V. Bazterra,⁴⁹ S. Beale,⁶
A. Bean,⁵⁶ M. Begalli,³ M. Biegel,⁷¹ C. Belanger-Champagne,⁴¹ L. Bellantoni,⁴⁸ S.B. Beri,²⁷ G. Bernardi,¹⁷
R. Bernhard,²² I. Bertram,⁴² M. Besançon,¹⁸ R. Beuselinck,⁴³ V.A. Bezzubov,³⁸ P.C. Bhat,⁴⁸ V. Bhatnagar,²⁷
G. Blazey,⁵⁰ S. Blessing,⁴⁷ K. Bloom,⁶⁴ A. Boehnlein,⁴⁸ D. Boline,⁷⁰ T.A. Bolton,⁵⁷ E.E. Boos,³⁷ G. Borissov,⁴²
T. Bose,⁵⁹ A. Brandt,⁷⁶ O. Brandt,²³ R. Brock,⁶² G. Brooijmans,⁶⁸ A. Bross,⁴⁸ D. Brown,¹⁷ J. Brown,¹⁷ X.B. Bu,⁴⁸
M. Buehler,⁷⁹ V. Buescher,²⁴ V. Bunichev,³⁷ S. Burdin^{b,42} T.H. Burnett,⁸⁰ C.P. Buszello,⁴¹ B. Calpas,¹⁵
E. Camacho-Pérez,³² M.A. Carrasco-Lizarraga,⁵⁶ B.C.K. Casey,⁴⁸ H. Castilla-Valdez,³² S. Chakrabarti,⁷⁰
D. Chakraborty,⁵⁰ K.M. Chan,⁵⁴ A. Chandra,⁷⁸ G. Chen,⁵⁶ S. Chevalier-Théry,¹⁸ D.K. Cho,⁷⁵ S.W. Cho,³¹
S. Choi,³¹ B. Choudhary,²⁸ T. Christoudias,⁴³ S. Cihangir,⁴⁸ D. Claes,⁶⁴ J. Clutter,⁵⁶ M. Cooke,⁴⁸ W.E. Cooper,⁴⁸
M. Corcoran,⁷⁸ F. Couderc,¹⁸ M.-C. Cousinou,¹⁵ A. Croc,¹⁸ D. Cutts,⁷⁵ A. Das,⁴⁵ G. Davies,⁴³ K. De,⁷⁶
S.J. de Jong,³⁴ E. De La Cruz-Burelo,³² F. Déliot,¹⁸ M. Demarteau,⁴⁸ R. Demina,⁶⁹ D. Denisov,⁴⁸ S.P. Denisov,³⁸
S. Desai,⁴⁸ K. DeVaughan,⁶⁴ H.T. Diehl,⁴⁸ M. Diesburg,⁴⁸ A. Dominguez,⁶⁴ T. Dorland,⁸⁰ A. Dubey,²⁸
L.V. Dudko,³⁷ D. Duggan,⁶⁵ A. Duperrin,¹⁵ S. Dutt,²⁷ A. Dyshkant,⁵⁰ M. Eads,⁶⁴ D. Edmunds,⁶² J. Ellison,⁴⁶
V.D. Elvira,⁴⁸ Y. Enari,¹⁷ H. Evans,⁵² A. Evdokimov,⁷¹ V.N. Evdokimov,³⁸ G. Facini,⁶⁰ T. Ferbel,⁶⁹ F. Fiedler,²⁴
F. Filthaut,³⁴ W. Fisher,⁶² H.E. Fisk,⁴⁸ M. Fortner,⁵⁰ H. Fox,⁴² S. Fuess,⁴⁸ T. Gadfort,⁷¹ A. Garcia-Bellido,⁶⁹
V. Gavrilov,³⁶ P. Gay,¹³ W. Geist,¹⁹ W. Geng,^{15,62} D. Gerbaudo,⁶⁶ C.E. Gerber,⁴⁹ Y. Gershtein,⁶⁵ G. Ginther,^{48,69}
G. Golovanov,³⁵ A. Goussiou,⁸⁰ P.D. Grannis,⁷⁰ S. Greder,¹⁹ H. Greenlee,⁴⁸ Z.D. Greenwood,⁵⁸ E.M. Gregores,⁴
G. Grenier,²⁰ Ph. Gris,¹³ J.-F. Grivaz,¹⁶ A. Grohsjean,¹⁸ S. Grünendahl,⁴⁸ M.W. Grünewald,³⁰ T. Guillemin,¹⁶
F. Guo,⁷⁰ G. Gutierrez,⁴⁸ P. Gutierrez,⁷³ A. Haas^{c,68} S. Hagopian,⁴⁷ J. Haley,⁶⁰ L. Han,⁷ K. Harder,⁴⁴ A. Harel,⁶⁹
J.M. Hauptman,⁵⁵ J. Hays,⁴³ T. Head,⁴⁴ T. Hebbeker,²¹ D. Hedin,⁵⁰ H. Hegab,⁷⁴ A.P. Heinson,⁴⁶ U. Heintz,⁷⁵
C. Hensel,²³ I. Heredia-De La Cruz,³² K. Herner,⁶¹ G. Hesketh^{d,44} M.D. Hildreth,⁵⁴ R. Hirosky,⁷⁹ T. Hoang,⁴⁷
J.D. Hobbs,⁷⁰ B. Hoeneisen,¹² M. Hohlfield,²⁴ Z. Hubacek,^{10,18} N. Huske,¹⁷ V. Hynek,¹⁰ I. Iashvili,⁶⁷
R. Illingworth,⁴⁸ A.S. Ito,⁴⁸ S. Jabeen,⁷⁵ M. Jaffré,¹⁶ D. Jamin,¹⁵ A. Jayasinghe,⁷³ R. Jesik,⁴³ K. Johns,⁴⁵
M. Johnson,⁴⁸ D. Johnston,⁶⁴ A. Jonckheere,⁴⁸ P. Jonsson,⁴³ J. Joshi,²⁷ A. Juste,⁴⁰ K. Kaadze,⁵⁷ E. Kajfasz,¹⁵
D. Karmanov,³⁷ P.A. Kasper,⁴⁸ I. Katsanos,⁶⁴ R. Kehoe,⁷⁷ S. Kermiche,¹⁵ N. Khalatyan,⁴⁸ A. Khanov,⁷⁴
A. Kharchilava,⁶⁷ Y.N. Khazheev,³⁵ D. Khatidze,⁷⁵ M.H. Kirby,⁵¹ J.M. Kohli,²⁷ A.V. Kozelov,³⁸ J. Kraus,⁶²
S. Kulikov,³⁸ A. Kumar,⁶⁷ A. Kupco,¹¹ T. Kurča,²⁰ V.A. Kuzmin,³⁷ J. Kvita,⁹ S. Lammers,⁵² G. Landsberg,⁷⁵
P. Lebrun,²⁰ H.S. Lee,³¹ S.W. Lee,⁵⁵ W.M. Lee,⁴⁸ J. Lellouch,¹⁷ L. Li,⁴⁶ Q.Z. Li,⁴⁸ S.M. Lietti,⁵ J.K. Lim,³¹
D. Lincoln,⁴⁸ J. Linnemann,⁶² V.V. Lipaev,³⁸ R. Lipton,⁴⁸ Y. Liu,⁷ Z. Liu,⁶ A. Lobodenko,³⁹ M. Lokajicek,¹¹
R. Lopes de Sa,⁷⁰ H.J. Lubatti,⁸⁰ R. Luna-Garcia^{e,32} A.L. Lyon,⁴⁸ A.K.A. Maciel,² D. Mackin,⁷⁸ R. Madar,¹⁸
R. Magaña-Villalba,³² S. Malik,⁶⁴ V.L. Malyshev,³⁵ Y. Maravin,⁵⁷ J. Martínez-Ortega,³² R. McCarthy,⁷⁰
C.L. McGivern,⁵⁶ M.M. Meijer,³⁴ A. Melnitchouk,⁶³ D. Menezes,⁵⁰ P.G. Mercadante,⁴ M. Merkin,³⁷ A. Meyer,²¹
J. Meyer,²³ F. Miconi,¹⁹ N.K. Mondal,²⁹ G.S. Muanza,¹⁵ M. Mulhearn,⁷⁹ E. Nagy,¹⁵ M. Naimuddin,²⁸ M. Narain,⁷⁵
R. Nayyar,²⁸ H.A. Neal,⁶¹ J.P. Negret,⁸ P. Neustroev,³⁹ S.F. Novaes,⁵ T. Nunnemann,²⁵ G. Obrant,³⁹ J. Orduna,⁷⁸
N. Osman,¹⁵ J. Osta,⁵⁴ G.J. Otero y Garzón,¹ M. Padilla,⁴⁶ A. Pal,⁷⁶ M. Pangilinan,⁷⁵ N. Parashar,⁵³
V. Parihar,⁷⁵ S.K. Park,³¹ J. Parsons,⁶⁸ R. Partridge^{c,75} N. Parua,⁵² A. Patwa,⁷¹ B. Penning,⁴⁸ M. Perfilov,³⁷
K. Peters,⁴⁴ Y. Peters,⁴⁴ K. Petridis,⁴⁴ G. Petrillo,⁶⁹ P. Pétrouff,¹⁶ R. Piegaia,¹ J. Piper,⁶² M.-A. Pleier,⁷¹
P.L.M. Podesta-Lerma^{f,32} V.M. Podstavkov,⁴⁸ M.-E. Pol,² P. Polozov,³⁶ A.V. Popov,³⁸ M. Prewitt,⁷⁸ D. Price,⁵²
N. Prokopenko,³⁸ S. Protopopescu,⁷¹ J. Qian,⁶¹ A. Quadt,²³ B. Quinn,⁶³ M.S. Rangel,² K. Ranjan,²⁸ P.N. Ratoff,⁴²
I. Razumov,³⁸ P. Renkel,⁷⁷ M. Rijssenbeek,⁷⁰ I. Ripp-Baudot,¹⁹ F. Rizatdinova,⁷⁴ M. Rominsky,⁴⁸ A. Ross,⁴²

45 C. Royon,¹⁸ P. Rubinov,⁴⁸ R. Ruchti,⁵⁴ G. Safronov,³⁶ G. Sajot,¹⁴ P. Salcido,⁵⁰ A. Sánchez-Hernández,³²
 46 M.P. Sanders,²⁵ B. Sanghi,⁴⁸ A.S. Santos,⁵ G. Savage,⁴⁸ L. Sawyer,⁵⁸ T. Scanlon,⁴³ R.D. Schamberger,⁷⁰
 47 Y. Scheglov,³⁹ H. Schellman,⁵¹ T. Schliephake,²⁶ S. Schlobohm,⁸⁰ C. Schwanenberger,⁴⁴ R. Schwienhorst,⁶²
 48 J. Sekaric,⁵⁶ H. Severini,⁷³ E. Shabalina,²³ V. Shary,¹⁸ A.A. Shchukin,³⁸ R.K. Shivpuri,²⁸ V. Simak,¹⁰
 49 V. Sirotenko,⁴⁸ P. Skubic,⁷³ P. Slattery,⁶⁹ D. Smirnov,⁵⁴ K.J. Smith,⁶⁷ G.R. Snow,⁶⁴ J. Snow,⁷² S. Snyder,⁷¹
 50 S. Söldner-Rembold,⁴⁴ L. Sonnenschein,²¹ K. Soustruznik,⁹ J. Stark,¹⁴ V. Stolin,³⁶ D.A. Stoyanova,³⁸ M. Strauss,⁷³
 51 D. Strom,⁴⁹ L. Stutte,⁴⁸ L. Suter,⁴⁴ P. Svoisky,⁷³ M. Takahashi,⁴⁴ A. Tanasijczuk,¹ W. Taylor,⁶ M. Titov,¹⁸
 52 V.V. Tokmenin,³⁵ Y.-T. Tsai,⁶⁹ D. Tsybychev,⁷⁰ B. Tuchming,¹⁸ C. Tully,⁶⁶ P.M. Tuts,⁶⁸ L. Uvarov,³⁹ S. Uvarov,³⁹
 53 S. Uzunyan,⁵⁰ R. Van Kooten,⁵² W.M. van Leeuwen,³³ N. Varelas,⁴⁹ E.W. Varnes,⁴⁵ I.A. Vasilyev,³⁸ P. Verdier,²⁰
 54 L.S. Vertogradov,³⁵ M. Verzocchi,⁴⁸ M. Vesterinen,⁴⁴ D. Vilanova,¹⁸ P. Vint,⁴³ P. Vokac,¹⁰ H.D. Wahl,⁴⁷
 55 M.H.L.S. Wang,⁶⁹ J. Warchol,⁵⁴ G. Watts,⁸⁰ M. Wayne,⁵⁴ M. Weber,^{9,48} L. Welty-Rieger,⁵¹ A. White,⁷⁶ D. Wicke,²⁶
 56 M.R.J. Williams,⁴² G.W. Wilson,⁵⁶ M. Wobisch,⁵⁸ D.R. Wood,⁶⁰ T.R. Wyatt,⁴⁴ Y. Xie,⁴⁸ C. Xu,⁶¹ S. Yacoob,⁵¹
 57 R. Yamada,⁴⁸ W.-C. Yang,⁴⁴ T. Yasuda,⁴⁸ Y.A. Yatsunenko,³⁵ Z. Ye,⁴⁸ H. Yin,⁴⁸ K. Yip,⁷¹ S.W. Youn,⁴⁸
 58 J. Yu,⁷⁶ S. Zelitch,⁷⁹ T. Zhao,⁸⁰ B. Zhou,⁶¹ J. Zhu,⁶¹ M. Zielinski,⁶⁹ D. Zieminska,⁵² and L. Zivkovic⁷⁵

(The D0 Collaboration*)

¹Universidad de Buenos Aires, Buenos Aires, Argentina

²LAFEX, Centro Brasileiro de Pesquisas Físicas, Rio de Janeiro, Brazil

³Universidade do Estado do Rio de Janeiro, Rio de Janeiro, Brazil

⁴Universidade Federal do ABC, Santo André, Brazil

⁵Instituto de Física Teórica, Universidade Estadual Paulista, São Paulo, Brazil

⁶Simon Fraser University, Vancouver, British Columbia, and York University, Toronto, Ontario, Canada

⁷University of Science and Technology of China, Hefei, People's Republic of China

⁸Universidad de los Andes, Bogotá, Colombia

⁹Charles University, Faculty of Mathematics and Physics,

Center for Particle Physics, Prague, Czech Republic

¹⁰Czech Technical University in Prague, Prague, Czech Republic

¹¹Center for Particle Physics, Institute of Physics,

Academy of Sciences of the Czech Republic, Prague, Czech Republic

¹²Universidad San Francisco de Quito, Quito, Ecuador

¹³LPC, Université Blaise Pascal, CNRS/IN2P3, Clermont, France

¹⁴LPSC, Université Joseph Fourier Grenoble 1, CNRS/IN2P3,

Institut National Polytechnique de Grenoble, Grenoble, France

¹⁵CPPM, Aix-Marseille Université, CNRS/IN2P3, Marseille, France

¹⁶LAL, Université Paris-Sud, CNRS/IN2P3, Orsay, France

¹⁷LPNHE, Universités Paris VI and VII, CNRS/IN2P3, Paris, France

¹⁸CEA, Irfu, SPP, Saclay, France

¹⁹IPHC, Université de Strasbourg, CNRS/IN2P3, Strasbourg, France

²⁰IPNL, Université Lyon 1, CNRS/IN2P3, Villeurbanne, France and Université de Lyon, Lyon, France

²¹III. Physikalisches Institut A, RWTH Aachen University, Aachen, Germany

²²Physikalisches Institut, Universität Freiburg, Freiburg, Germany

²³II. Physikalisches Institut, Georg-August-Universität Göttingen, Göttingen, Germany

²⁴Institut für Physik, Universität Mainz, Mainz, Germany

²⁵Ludwig-Maximilians-Universität München, München, Germany

²⁶Fachbereich Physik, Bergische Universität Wuppertal, Wuppertal, Germany

²⁷Panjab University, Chandigarh, India

²⁸Delhi University, Delhi, India

²⁹Tata Institute of Fundamental Research, Mumbai, India

³⁰University College Dublin, Dublin, Ireland

³¹Korea Detector Laboratory, Korea University, Seoul, Korea

³²CINVESTAV, Mexico City, Mexico

³³FOM-Institute NIKHEF and University of Amsterdam/NIKHEF, Amsterdam, The Netherlands

³⁴Radboud University Nijmegen/NIKHEF, Nijmegen, The Netherlands

³⁵Joint Institute for Nuclear Research, Dubna, Russia

³⁶Institute for Theoretical and Experimental Physics, Moscow, Russia

³⁷Moscow State University, Moscow, Russia

³⁸Institute for High Energy Physics, Protvino, Russia

³⁹Petersburg Nuclear Physics Institute, St. Petersburg, Russia

⁴⁰Institució Catalana de Recerca i Estudis Avançats (ICREA) and Institut de Física d'Altes Energies (IFAE), Barcelona, Spain

⁴¹Stockholm University, Stockholm and Uppsala University, Uppsala, Sweden

⁴²Lancaster University, Lancaster LA1 4YB, United Kingdom

* with visitors from ^aAugustana College, Sioux Falls, SD, USA, ^bThe University of Liverpool, Liverpool, UK, ^cSLAC, Menlo Park, CA, USA, ^dUniversity College London, London, UK, ^eCentro de Investigacion en Computacion - IPN, Mexico City, Mexico, ^fECFM, Universidad Autonoma de Sinaloa, Culiacán, Mexico, and ^gUniversität Bern, Bern, Switzerland.

- 105 ⁴³Imperial College London, London SW7 2AZ, United Kingdom
 106 ⁴⁴The University of Manchester, Manchester M13 9PL, United Kingdom
 107 ⁴⁵University of Arizona, Tucson, Arizona 85721, USA
 108 ⁴⁶University of California Riverside, Riverside, California 92521, USA
 109 ⁴⁷Florida State University, Tallahassee, Florida 32306, USA
 110 ⁴⁸Fermi National Accelerator Laboratory, Batavia, Illinois 60510, USA
 111 ⁴⁹University of Illinois at Chicago, Chicago, Illinois 60607, USA
 112 ⁵⁰Northern Illinois University, DeKalb, Illinois 60115, USA
 113 ⁵¹Northwestern University, Evanston, Illinois 60208, USA
 114 ⁵²Indiana University, Bloomington, Indiana 47405, USA
 115 ⁵³Purdue University Calumet, Hammond, Indiana 46323, USA
 116 ⁵⁴University of Notre Dame, Notre Dame, Indiana 46556, USA
 117 ⁵⁵Iowa State University, Ames, Iowa 50011, USA
 118 ⁵⁶University of Kansas, Lawrence, Kansas 66045, USA
 119 ⁵⁷Kansas State University, Manhattan, Kansas 66506, USA
 120 ⁵⁸Louisiana Tech University, Ruston, Louisiana 71272, USA
 121 ⁵⁹Boston University, Boston, Massachusetts 02215, USA
 122 ⁶⁰Northeastern University, Boston, Massachusetts 02115, USA
 123 ⁶¹University of Michigan, Ann Arbor, Michigan 48109, USA
 124 ⁶²Michigan State University, East Lansing, Michigan 48824, USA
 125 ⁶³University of Mississippi, University, Mississippi 38677, USA
 126 ⁶⁴University of Nebraska, Lincoln, Nebraska 68588, USA
 127 ⁶⁵Rutgers University, Piscataway, New Jersey 08855, USA
 128 ⁶⁶Princeton University, Princeton, New Jersey 08544, USA
 129 ⁶⁷State University of New York, Buffalo, New York 14260, USA
 130 ⁶⁸Columbia University, New York, New York 10027, USA
 131 ⁶⁹University of Rochester, Rochester, New York 14627, USA
 132 ⁷⁰State University of New York, Stony Brook, New York 11794, USA
 133 ⁷¹Brookhaven National Laboratory, Upton, New York 11973, USA
 134 ⁷²Langston University, Langston, Oklahoma 73050, USA
 135 ⁷³University of Oklahoma, Norman, Oklahoma 73019, USA
 136 ⁷⁴Oklahoma State University, Stillwater, Oklahoma 74078, USA
 137 ⁷⁵Brown University, Providence, Rhode Island 02912, USA
 138 ⁷⁶University of Texas, Arlington, Texas 76019, USA
 139 ⁷⁷Southern Methodist University, Dallas, Texas 75275, USA
 140 ⁷⁸Rice University, Houston, Texas 77005, USA
 141 ⁷⁹University of Virginia, Charlottesville, Virginia 22901, USA
 142 ⁸⁰University of Washington, Seattle, Washington 98195, USA

We present a measurement of the $t\bar{t}$ production cross section in $p\bar{p}$ collisions at $\sqrt{s} = 1.96$ TeV using 5.4 fb^{-1} of data collected with the D0 detector. We consider decay channels with two electrons, two muons, or one electron and one muon in the final state. For a top quark mass of $m_t = 172.5$ GeV, the measured cross section is $7.4_{-0.8}^{+0.9}$ (stat + syst) pb. This result combined with the cross section measurement in the lepton + jets final state yields a cross section of 7.6 ± 0.6 (stat + syst) pb which agrees with the standard model expectation.

PACS numbers: 14.65.Ha, 13.85.Lg, 13.85.Qk, 14.60.Fg, 12.15.Ff

I. INTRODUCTION

Precisely measuring the top quark pair ($t\bar{t}$) production cross section ($\sigma_{t\bar{t}}$) and comparing such a measurement with the current predictions from the standard model (SM) provides an important test of perturbative quantum chromodynamics (QCD). At present, the most precise predictions of $\sigma_{t\bar{t}}$ are given by approximate next to next-to-leading order (NNLO) calculations [1–3] with a precision of 6% to 9% which challenges the experimental precision for the measurement of $\sigma_{t\bar{t}}$. Furthermore, because $\sigma_{t\bar{t}}$ depends on the top quark mass (m_t), it can be used to constrain that SM parameter [4, 5]. Comparing the SM prediction with the measured $\sigma_{t\bar{t}}$ value allows testing for the presence of physics beyond the SM, as for instance, scenarios in which the top quark would decay into a charged Higgs boson and a b quark [5].

In this letter we present an updated measurement of $\sigma_{t\bar{t}}$ in $p\bar{p}$ collisions at $\sqrt{s} = 1.96$ TeV in the dilepton ($\ell\ell'$) channel. In this channel, both W bosons from top quark decay leptonically into $e\nu_e$, $\mu\nu_\mu$, or $\tau\nu_\tau$. We consider only $\tau \rightarrow e\nu_e\nu_\tau$, $\tau \rightarrow \mu\nu_\mu\nu_\tau$ decays, thus giving rise to the ee , $\mu\mu$, or $e\mu$ final state. This measurement complements the

156 $\sigma_{t\bar{t}}$ measurements in the lepton+jets (ℓj) channel in which one of the W bosons decays hadronically into a $q\bar{q}'$ pair
 157 and the other W boson decays leptonically [6, 7], as well as measurements in the all-hadronic channel in which both
 158 W bosons decay hadronically [8].

159 The measurement is based on data collected with the D0 detector during Run II of the Fermilab Tevatron Collider
 160 that correspond to an integrated luminosity of $5.4 \pm 0.3 \text{ fb}^{-1}$. This result supersedes our previous measurement [9],
 161 which used a dataset five times smaller than the one considered here. The CDF Collaboration has performed a $\sigma_{t\bar{t}}$
 162 measurement in the $\ell\ell'$ channel using 2.8 fb^{-1} of data [10]. The ATLAS and CMS Collaborations recently published
 163 their first $\sigma_{t\bar{t}}$ measurements in pp collisions at $\sqrt{s} = 7 \text{ TeV}$ [11, 12].

164 The D0 detector is described in detail in [13]. The region of the D0 detector closest to the interaction point contains
 165 a tracking system consisting of a silicon microstrip tracker (SMT) and a central fiber tracker (CFT), both located
 166 inside a superconducting solenoid magnet which generates a magnetic field of 1.9 T. Hits in these two detectors are
 167 used to reconstruct tracks from charged particles in the pseudorapidity region $|\eta| < 3$ [28]. Surrounding the two
 168 tracking subdetectors are liquid-argon uranium calorimeters, segmented into electromagnetic and hadronic sections.
 169 The central section of the calorimeter (CC) covers pseudorapidities $|\eta| < 1.1$, and the two end calorimeters (EC)
 170 extend coverage to $|\eta| \approx 4.2$ with all three housed in separate cryostats. The muon system surrounds the calorimeter
 171 and consists of three layers of tracking detectors and scintillator trigger counters covering $|\eta| < 2$. A toroidal iron
 172 magnet with a field of 1.8 T is located outside the innermost layer of the muon detector. The luminosity is calculated
 173 from the rate of inelastic $p\bar{p}$ collisions measured with plastic scintillator arrays located in front of the EC cryostats [14].

174 The D0 trigger is based on a three-level pipeline system. The first level is implemented in custom-designed hardware.
 175 The second level uses high-level processors to combine information from the different sub-detectors to construct simple
 176 physics objects. The software-based third level uses full event information obtained with a simplified reconstruction
 177 algorithm.

178 II. OBJECT IDENTIFICATION

179 The $t\bar{t}$ dilepton final state contains two leptons (electrons, muons or an electron and a muon), at least two jets, and
 180 significant missing transverse momentum (\cancel{p}_T).

181 Electrons are identified as energy clusters with radius $R = \sqrt{\Delta\eta^2 + \Delta\phi^2} < 0.2$ in the calorimeter which are
 182 consistent in their profile with that of an electromagnetic shower. More than 90% of the energy of the electron
 183 candidate must be deposited in the electromagnetic part of the calorimeter, and less than 20% of its energy may
 184 be deposited in a calorimeter annulus of $0.2 < R < 0.4$ around its direction. This cluster has to be matched to a
 185 track. We consider electrons in the CC with $|\eta| < 1.1$ and in the EC with $1.5 < |\eta| < 2.5$. Additionally, we require
 186 an electron likelihood discriminant based on tracking and calorimeter information to be larger than 0.85. Electrons
 187 fulfilling all these cuts are called tight electrons.

188 A muon is identified as a segment in at least one layer of the outer muon chambers in the full acceptance of the
 189 D0 muon system that is matched to a track in the central tracking system. Reconstructed muons must satisfy two
 190 isolation criteria. First, the transverse energy deposited in a calorimeter annulus around the muon $0.1 < R < 0.4$
 191 ($E_T^{\mu \text{ iso}}$) has to be less than 15% of the transverse momentum of the muon (p_T^μ). Second, the sum of the p_{TS} of the
 192 tracks in a cone of radius $R < 0.5$ around the muon track in the central tracking system ($p_T^{\mu \text{ iso}}$) has to be less than
 193 15% of p_T^μ . Muons that fulfill these isolation criteria are referred to as tight isolated muons.

194 For events simulated by Monte Carlo (MC), the residual differences with data in the electron and muon
 195 p_T resolutions and in the electron and muon identification efficiencies are corrected. These corrections are derived by
 196 measuring the efficiencies and resolutions in $Z/\gamma^* \rightarrow \ell\ell$ data and in MC events, identifying one tight lepton as a tag
 197 and using the other charged lepton as a probe (tag-and-probe method).

198 Jets are identified with a fixed cone algorithm with radius $R < 0.5$ [15] in the range $|\eta| < 2.5$. A jet energy
 199 scale correction (JES) is determined by calibrating the energy deposited in the jet cone using transverse momentum
 200 balance in γ +jet and dijet events. If a muon overlaps with the jet cone, the momentum of that muon is included in
 201 the correction to account for the energy lost to semileptonic hadron decays.

202 We require that the jets be matched to at least two tracks originating from the vertex of the primary interaction
 203 (PV). Jets in MC are corrected for the residual differences between data and MC in the energy resolution and JES.
 204 These correction factors are measured by comparing data and MC in $(Z/\gamma^* \rightarrow ee)$ +jets events.

205 We use a neural-network (NN) tagging algorithm [16] to identify jets from b quarks. The algorithm combines
 206 information from the impact parameters of the tracks and variables that characterize the presence and properties of
 207 secondary vertices within the jet. In order to use this information for b tagging, the jet is required to be matched to
 208 a jet built from tracks. Jets fulfilling this requirement are called taggable jets.

209 The \cancel{p}_T is reconstructed from the energy deposited in the calorimeter cells. Correction for lepton and jet p_{TS} are
 210 propagated into the \cancel{p}_T . The missing transverse momentum significance ($\sigma_{\cancel{p}_T}$) is defined in each event as the \cancel{p}_T

211 divided by its uncertainty.

212 More details about object identification can be found in [17].

213 III. EVENT SELECTION AND BACKGROUND ESTIMATION

214 The main sources of background in the $\ell\ell'$ channel come from Drell-Yan and Z boson production ($Z/\gamma^* \rightarrow \ell\ell$),
215 diboson production (WW, WZ, ZZ), and instrumental background. The instrumental background mainly arises from
216 multijet and W +jets events in which one or two jets are misidentified as electrons or an isolated muon originating
217 from the semileptonic decay of a heavy flavor quark is emitted by jet.

218 For this analysis we consider events that fired a set of single lepton triggers for the ee and $\mu\mu$ channels. For the $e\mu$
219 channel, we consider events selected by any trigger. Efficiencies for single lepton triggers have been measured using
220 the tag-and-probe method with $Z/\gamma^* \rightarrow \ell\ell$ data. These efficiencies are found to be around 99% for the ee channel and
221 80% for the $\mu\mu$ final state. For the $e\mu$ channel the overall efficiency of the single lepton and electron-muon triggers is
222 close to 100%.

223 In order to separate $t\bar{t}$ signal events from background, the following selection is applied:

- 224 • We require at least one PV in the beam interaction region with $|z| < 60$ cm, where z is the coordinate along the
225 beam axis and $z = 0$ in the center of the detector. At least three tracks must be associated with this PV.
- 226 • We require at least two isolated leptons with $p_T > 15$ GeV. These two leptons must originate from the same
227 PV, i.e. the difference between the z coordinates of the two lepton tracks should be less than 2 cm, where the z
228 coordinate is calculated at the point of the track's closest approach to the beam.
- 229 • We require the two selected leptons to have opposite charge.
- 230 • In the $e\mu$ final state, we require the distance between the electron and the muon directions $R(e, \mu) > 0.3$ to
231 reduce the background from bremsstrahlung.
- 232 • We require at least two jets with $p_T > 20$ GeV. In the $e\mu$ channel, we also consider events with only one jet.
- 233 • To further improve the signal purity of the selected sample, we apply additional topological selections. In the $e\mu$
234 final state with two jets, we require $H_T > 110$ GeV, where H_T is the scalar sum of the transverse momenta of
235 the leading lepton and the two leading jets. In the $e\mu$ channel with exactly one jet, we require $H_T > 105$ GeV.
236 In the ee final state, we require $\sigma_{p_T} > 5$ while in the $\mu\mu$ channel we require $\cancel{p}_T > 40$ GeV and $\sigma_{\cancel{p}_T} > 5$.

237 In order to estimate the signal efficiency and the background contamination, we use the MC simulation for all
238 contributions but the instrumental background, the latter being derived from data. The $t\bar{t}$ and Z/γ^* events are
239 generated with the tree level matrix element generator ALPGEN [18] interfaced with the PYTHIA [19] generator for
240 parton showering and hadronization. Diboson events are generated with PYTHIA. All simulated samples are generated
241 using the CTEQ6L1 parton distribution functions (PDFs) [20]. The Z/γ^* samples are normalized to the NNLO cross
242 section computed for different dilepton invariant mass ranges with the FEWZ program [21]. We separately simulate
243 Z/γ^* with heavy flavor (HF) quarks $Z/\gamma^* + b\bar{b}$ (or $Z/\gamma^* + c\bar{c}$) using ALPGEN and enhance the corresponding leading
244 order cross sections by a factor of 1.5 (1.7) estimated with the MCFM program [22]. The diboson samples are normalized
245 to the next-to-leading order cross section calculated with MCFM. Uncertainties in these normalization factors are taken
246 into account as systematic uncertainties. We additionally apply a correction to the Z/γ^* +jets simulation to address
247 the imperfect modeling of the Z boson p_T in the MC.

248 The instrumental background is estimated directly from data. First, in the ee and $e\mu$ channels we determine
249 the contribution of events with jets misidentified as electrons using the signal data sample but without the electron
250 likelihood discriminant cut. We extract the number of events with misidentified jets, n_f , and the number of events
251 with real electrons, n_e , by fitting the electron likelihood distribution with an extended likelihood fit, using the following
252 likelihood function:

$$\mathcal{L} = \prod_{i=1}^N [n_e S(x_i) + n_f B(x_i)] \frac{e^{-n_e + n_f}}{N!}, \quad (1)$$

253 where N is the number of selected events, and $S(x_i)$ and $B(x_i)$ are the signal and background probability density
254 functions (pdfs), and i runs over all selected events. The signal pdf is measured in $Z/\gamma^* \rightarrow ee$ data events. The
255 background pdf is measured in $e\mu$ events with the same selection as the analysis sample but inverting the opposite
256 sign lepton requirement (same sign sample) without any topological requirement but with muon anti-isolation cuts:
257 $E_T^{\mu \text{ iso}}/p_T^{\mu} > 0.2$ and $p_T^{\mu \text{ iso}}/p_T^{\mu} > 0.2$. The total number of events with a jet misidentified as an electron in the signal
258 selection can be found as $n = n_f \int_{0.85}^{1.0} B(x) dx$, where the integration is done over the high likelihood region. The

TABLE I: Numbers of expected and observed events assuming the SM $t\bar{t}$ cross section for a top quark mass of $m_t = 172.5$ GeV (7.45 pb). The expected numbers of events is shown with its statistical and systematic uncertainties. The uncertainty on the ratio between observed and expected numbers of events takes into account the statistical uncertainty in the observed number of events and the systematic uncertainty in the expected number of events.

Channel	$Z \rightarrow \ell\ell$	Diboson	Instrumental background	$t\bar{t} \rightarrow \ell\bar{\ell}b\bar{b}\nu\bar{\nu}$	Expected N of events	Observed N of events	Observed Expected
$e\mu$ two jets	30.3 ± 4.2	8.6 ± 1.2	22.7 ± 8.6	191.5 ± 18.8	253.1 ± 24.3	281	1.11 ± 0.13
$e\mu$ one jet	40.9 ± 4.8	20.7 ± 2.4	25.3 ± 10.5	52.1 ± 9.4	139.0 ± 16.5	150	1.08 ± 0.16
ee	12.6 ± 2.0	3.0 ± 0.4	-	45.6 ± 5.3	61.1 ± 7.1	74	1.21 ± 0.20
$\mu\mu$	67.3 ± 9.7	5.1 ± 0.7	7.6 ± 1.2	59.8 ± 6.6	139.8 ± 15.7	144	1.03 ± 0.14

estimation is performed separately in CC and EC. We find that the contribution of instrumental background to the ee channel is negligible.

In a second step, we determine the number of events with an isolated muon arising from jets in the $e\mu$ and $\mu\mu$ channels. This number is estimated as $n_f^\mu = N_{\text{loose}} f_\mu$, where N_{loose} is the number of events in the same sign sample with loose isolation criteria on the muon: $E_T^{\mu \text{ iso}}/p_T^\mu < 0.5$ and $p_T^{\mu \text{ iso}}/p_T^\mu < 0.5$. In the $\mu\mu$ final state, we apply these loose isolation cuts only to one randomly chosen muon. In the $e\mu$ channel, the number of events with jets misidentified as electrons in the same sign sample is subtracted from N_{loose} . The muon misidentified isolation rate f_μ is determined in a dimuon sample with at least one jet. In this sample we require one muon to be close to the jet ($dR(\mu, \text{jet}) < 0.5$) with anti-isolation cuts $E_T^{\mu \text{ iso}}/p_T^\mu > 0.15$ and $p_T^{\mu \text{ iso}}/p_T^\mu > 0.15$. The other muon defined as the probe should pass the loose isolation cuts $E_T^{\mu \text{ iso}}/p_T^\mu < 0.5$ and $p_T^{\mu \text{ iso}}/p_T^\mu < 0.5$. We compute f_μ as the ratio of the number of events in which the probe muon passes the tight isolation cuts to the total number of events in this same sign sample.

The number of predicted background events as well as the expected number of signal events in the four channels are shown in Table I. In order to achieve a better separation between signal and background when measuring the cross section, we use the distribution of the smallest of the two b -tagging NN discriminant outputs of the two leading jets. These NN discriminant distributions for the different channels are shown in Fig. 1. We measure the $t\bar{t}$ cross section $\sigma_{t\bar{t}}$ by simultaneously fitting the NN distributions in the four channels and maximizing the following likelihood function:

$$\mathcal{L} = \prod_{i=1}^{i \leq 4} \prod_{j=1}^{j \leq 14} P[n_{ij}, \mu_{ij}(\sigma_{t\bar{t}})], \quad (2)$$

where i runs over the channels and j over the bins of the NN distribution, $P[n, \mu(\sigma_{t\bar{t}})]$ is the Poisson probability function to observe n events when $\mu(\sigma_{t\bar{t}})$ events are expected.

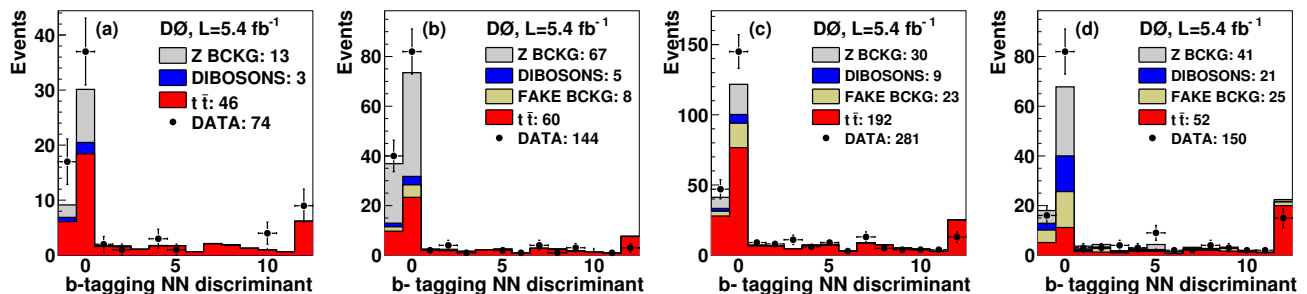


FIG. 1: Expected and observed distributions for the smallest b -tagging NN discriminant outputs of the two leading jets for the (a) ee channel, (b) $\mu\mu$ channel, (c) $e\mu$ channel, and (d) $e\mu$ one jet channel. The $t\bar{t}$ signal is normalized to the SM cross section (7.45 pb). The x axis represents the NN output non-uniformly mapped to 14 bins. The bin with central value 0 represents the lowest probability for a jet to be produced by a b quark. The bin with value 12 represents the highest probability. The bin with value -1 represents the jets which do not satisfy the requirements to enter the NN computation (non-taggable jets).

IV. RESULTS AND UNCERTAINTIES

The main systematic uncertainties for the measurement of the $t\bar{t}$ cross section are described in the following. The uncertainty in the measured integrated luminosity of 6.1% [14] directly affects the cross section measurement and also the expected numbers of Z/γ^* and diboson background events. Uncertainties in lepton identification efficiencies are determined by evaluating the different sources of bias in the tag-and-probe method and data/MC differences in $Z/\gamma^* \rightarrow \ell\ell$ events. Uncertainties in the lepton energy resolution are determined by comparing the width of the Z boson invariant mass distributions in data and MC.

The uncertainty in the relative JES between data and MC for light quark jets is measured in $Z/\gamma^* + \text{jets}$ events. The uncertainty on the difference between the light and b quark JESs (1.8%) is estimated by propagating the difference in the single pion response between data and MC to the MC JES for b quark jets. Jet energy resolution uncertainties are estimated by comparing the resolutions measured in $Z/\gamma^* + \text{jets}$ events in data and in MC. The uncertainty on the jet identification efficiency is estimated by comparing the efficiencies measured in dijet events for data and MC. The b quark identification uncertainties include uncertainties in the probability of tagging a b quark jet, the probability of tagging a light quark jet or gluon, and the probability for a jet not to be taggable [16].

To estimate the uncertainty in the trigger efficiency, we use events selected with the same criteria as the $t\bar{t}$ signal but without any jet requirement. In all four channels this selection is dominated by Z/γ^* events. We compute the ratio of the expected and observed number of events for two cases: when both leptons are allowed to fire the trigger or when only one lepton is allowed to fire the trigger. The difference in these ratios is used to estimate the uncertainty on the trigger efficiency.

Several uncertainties on the signal modeling are considered. The effects of higher order corrections and the hadronization modeling are estimated as the difference in signal efficiencies using the default ALPGEN+ PYTHIA simulation and using events generated with the MC@NLO [23] generator. The uncertainty coming from color reconnection is evaluated by comparing the $t\bar{t}$ efficiency using PYTHIA v6.4 tune Apro and PYTHIA v6.4 tune ACRpro [24]. The uncertainty on initial (ISR) and final (FSR) state radiation is evaluated by varying the ISR/FSR parameters in PYTHIA and evaluating the change in the signal efficiency. The uncertainty due to PDFs is estimated by reweighting the signal efficiency to the CTEQ6.1M PDFs [25] and looking at the efficiency variation along the 20 pairs of CTEQ6.1M eigenvector uncertainties. The uncertainty due to the simulation of b quark fragmentation is assigned to be the difference between tuning the parameters of the b quark fragmentation function to LEP or SLD data [26].

The uncertainty in the background normalization includes the theoretical uncertainties in the cross section and the uncertainty due to the correction for the Z boson p_T modeling. We also take into account an uncertainty due to the limited statistics of the signal and background templates of the NN discriminant. For the following systematic uncertainties, we take into account the shape changing effects of the b -tagging NN output discriminant: jet energy scale, jet resolution, jet identification, and b quark identification uncertainties.

Maximizing the likelihood function in Eq. 2 and using the above systematic uncertainties, we measure the $t\bar{t}$ cross section for a top quark mass of $m_t = 172.5$ GeV and find

$$\sigma_{t\bar{t}} = 8.0 \pm 0.5 \text{ (stat)} \pm 1.0 \text{ (syst)} \text{ pb.} \quad (3)$$

In order to reduce the influence of systematic uncertainties on the cross section measurement, we use the nuisance parameters technique [27] to constrain the overall uncertainty using the data NN output distribution itself. Using this technique, the likelihood (Eq. 2) has to be modified to be

$$\mathcal{L} = \prod_{i=1}^{i \leq 4} \prod_{j=1}^{j \leq 14} P[n_{ij}, \mu_{ij}(\sigma_{t\bar{t}})] \prod_k \mathcal{G}(\nu_k; 0, SD). \quad (4)$$

The impact of each uncertainty k is parameterized by a nuisance parameter ν_k that is constrained with a Gaussian probability \mathcal{G} with a mean of zero and a width corresponding to the size (SD) of the uncertainty. Correlations of systematic uncertainties between channels and between the different samples are naturally taken into account by assigning the same nuisance parameter to the correlated systematic uncertainty. In Eq. 4, the free parameters of the fit are ν_k and $\sigma_{t\bar{t}}$.

As can be seen from Eq. 3, the systematic uncertainties are the limiting uncertainties in the precision of the $t\bar{t}$ cross section measurement. Varying the systematic uncertainties and constraining them with data using the nuisance parameter technique can therefore significantly improve the measurement. Using the nuisance parameter technique we find an improved overall uncertainty of approximately 20% and reach a relative precision of 11% in the $t\bar{t}$ cross section:

$$\sigma_{t\bar{t}} = 7.4_{-0.8}^{+0.9} \text{ (stat + syst)} \text{ pb}$$

for $m_t = 172.5$ GeV. The uncertainties in this measurement are summarized in Table II. For each category of systematic uncertainty listed in Table II, only the corresponding nuisance parameters are allowed to vary. The absolute shift of the measured $t\bar{t}$ cross section with respect to the result obtained including only statistical uncertainties is shown in the column “Offset.” In the columns “ $+\sigma$ ” and “ $-\sigma$,” the positive and negative systematic uncertainties on the measured cross section for each category are listed. The line “Fit result” contains the result of the full nuisance parameter fit, where all nuisance parameters are allowed to vary at the same time, which can result in a different “offset” and different uncertainties in the final $t\bar{t}$ cross section than expected from the sum of the individual “offsets” and systematic uncertainties. The uncertainty quoted in this line includes the full statistical and systematic uncertainty on the result.

TABLE II: Measured $t\bar{t}$ cross section with the breakdown of uncertainties in the $\ell\ell'$ channel and for the combined $\ell\ell'$ and ℓj measurement using the nuisance parameter technique. The offsets show how the mean value of the measured cross section is shifted due to each source of systematic uncertainty. In each line, all but the considered source of systematic uncertainty are ignored. The $\pm\sigma$ give the impact on the measured cross section when the nuisance parameters describing the considered category are changed by ± 1 SD of their fitted value. See text for further details.

Source	$\ell\ell'$				$\ell\ell'+\ell j$				
	$\sigma_{t\bar{t}}$ [pb]	Offset [pb]	$+\sigma$ [pb]	$-\sigma$ [pb]	$\sigma_{t\bar{t}}$ [pb]	Offset [pb]	$+\sigma$ [pb]	$-\sigma$ [pb]	
Statistical only	8.05		+0.50	-0.48	7.72		+0.20	-0.20	
Muon identification		+0.00	+0.13	-0.12		-0.06	+0.06	-0.06	
Electron identification and smearing		-0.23	+0.28	-0.25		+0.05	+0.13	-0.13	
Signal modeling		-0.02	+0.40	-0.35		-0.11	+0.16	-0.15	
Triggers		+0.00	+0.00	-0.00		-0.09	+0.10	-0.10	
Jet energy scale		-0.16	+0.16	-0.15		-0.01	+0.03	-0.03	
Jet reconstruction and identification		-0.21	+0.24	-0.22		+0.24	+0.08	-0.08	
b -tagging		+0.14	+0.00	+0.00		-0.04	+0.16	-0.12	
Background normalization		-0.21	+0.26	-0.24		-0.05	+0.11	-0.10	
W +HF fraction		-	-	-		-0.01	+0.11	-0.11	
Instrumental background		-0.11	+0.19	-0.19		-0.02	+0.05	-0.05	
Luminosity		-0.69	+0.58	-0.51		-0.45	+0.44	-0.40	
Other		-0.04	+0.12	-0.11		-0.01	+0.13	-0.12	
Template statistics		+0.00	+0.09	+0.09		+0.00	+0.04	-0.04	
Total systematics			-1.51	+0.89			-0.55	+0.58	+0.52
Fit result	7.38		+0.89	-0.78	7.55		+0.62	-0.56	

Furthermore, we combine this measurement with the cross section measurement in the fully orthogonal ℓj channel [6] using the same nuisance parameter approach and taking all correlations into account. In the ℓj channel, the events are separated into events with three or at least four jets, of which zero, one, or at least two jets are b -tagged. In events that have three or four jets but no b -tagged jets or events with three jets and one b -tagged jet, we use a topological discriminant to improve the separation of signal and background. In [6] the separation into these channels and application of topological methods is referred to as the combined method. For this combination, we did not simultaneously fit the heavy flavor fraction for W +jet processes (W +HF) in the ℓj channel as was done in [6], making it unnecessary to use ℓj events with only two jets. With this change compared to [6], the measured ℓj $t\bar{t}$ cross section for $m_t = 172.5$ GeV is

$$\sigma_{t\bar{t}} = 7.9_{-0.7}^{+0.8} (\text{stat} + \text{syst}) \text{ pb.}$$

The combination of the measurements in the $\ell\ell'$ and ℓj final states is done by maximizing the product of the likelihood function for dilepton Eq. 2 and the likelihood function of the ℓj channel [6], which yields

$$\sigma_{t\bar{t}} = 7.6 \pm 0.6 (\text{stat} + \text{syst}) \text{ pb}$$

for $m_t = 172.5$ GeV. This combination has a relative precision of 8% and represents an improvement of about 12% relative to the ℓj cross section measurement alone. The uncertainties for this combined measurement are summarized in Table II.

Due to acceptance effects, the $t\bar{t}$ efficiency depends on the assumed top quark mass in the MC. We extract the $t\bar{t}$ cross section using simulated $t\bar{t}$ events with different values of m_t . The resulting cross sections can be fitted with the following functional form:

$$\sigma_{t\bar{t}}(m_t) = \frac{1}{m_t^4} [a + b(m_t - 170 \text{ GeV})]$$

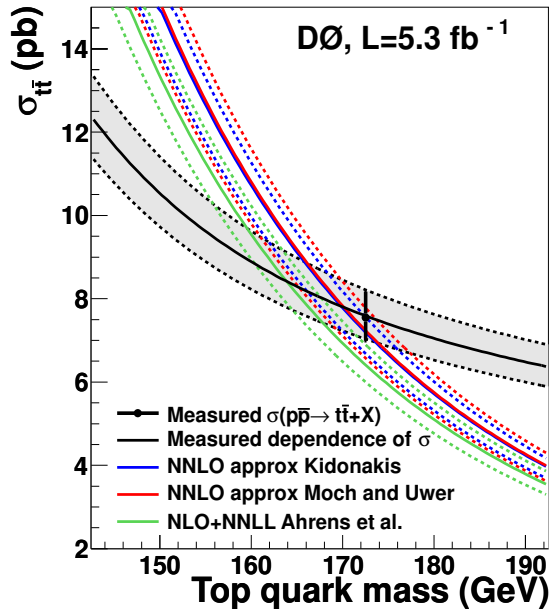


FIG. 2: Dependence of the experimental and theoretical [1–3] $t\bar{t}$ cross sections on the top quark mass. The point shows the combined $\ell\ell'$ and ℓj cross section measurement for $m_t = 172.5$ GeV.

$$+ c(m_t - 170 \text{ GeV})^2 + d(m_t - 170 \text{ GeV})^3 \text{ pb}, \quad (5)$$

with $a = 6.51782 \times 10^9 \text{ GeV}^4$, $b = 7.8843 \times 10^7 \text{ GeV}^3$, $c = 9.30691 \times 10^5 \text{ GeV}^2$, and $d = -2.421 \times 10^3 \text{ GeV}$ and where $\sigma_{t\bar{t}}$ and m_t are in pb and GeV, respectively. Figure 2 shows this parameterization for the measurement as a function of top quark mass together with approximate NNLO computations [1–3].

V. CONCLUSION

In this letter we presented an updated measurement of the $t\bar{t}$ production cross section in the dilepton final state using 5.4 fb^{-1} of data. This cross section measurement yields $7.4_{-0.8}^{+0.9}$ (stat + syst) pb and has a relative precision of $+12\%$ / -11% . It is currently the most precise measurement of the $t\bar{t}$ cross section in the dilepton channel. Combining this measurement in the dilepton channel with our result in the lepton + jets channel [6] yields 7.6 ± 0.6 (stat + syst) pb which corresponds to a relative precision of 8%. This measurement is in good agreement with the SM prediction.

We thank the staffs at Fermilab and collaborating institutions, and acknowledge support from the DOE and NSF (USA); CEA and CNRS/IN2P3 (France); FASI, Rosatom and RFBR (Russia); CNPq, FAPERJ, FAPESP and FUNDUNESP (Brazil); DAE and DST (India); Colciencias (Colombia); CONACyT (Mexico); KRF and KOSEF (Korea); CONICET and UBACyT (Argentina); FOM (The Netherlands); STFC and the Royal Society (United Kingdom); MSMT and GACR (Czech Republic); CRC Program and NSERC (Canada); BMBF and DFG (Germany); SFI (Ireland); The Swedish Research Council (Sweden); and CAS and CNSF (China).

-
- [1] V. Ahrens, A. Ferroglia, M. Neubert, B. D. Pecjak, and L. L. Yang, *J. High Energy Phys.* **1009**, 097 (2010); V. Ahrens, A. Ferroglia, M. Neubert, B. D. Pecjak, and L. L. Yang, *Nucl. Phys. Proc. Suppl.* **205–206**, 48 (2010).
[2] S. Moch and P. Uwer, *Phys. Rev. D* **78**, 034003 (2008); U. Langenfeld, S. Moch, and P. Uwer, *Phys. Rev. D* **80**, 054009 (2009).
[3] N. Kidonakis and R. Vogt, *Phys. Rev. D* **68**, 114014 (2003); N. Kidonakis, *Phys. Rev. D* **82**, 114030 (2010).
[4] V. M. Abazov *et al.* (D0 Collaboration), *Phys. Lett. B* **679**, 177 (2009).
[5] V. M. Abazov *et al.* (D0 Collaboration), *Phys. Rev. D* **80**, 071102 (2009).
[6] V. M. Abazov *et al.* (D0 Collaboration), arXiv:1101.0124, submitted to *Phys. Rev. D*.

- 374 [7] V. M. Abazov *et al.* (D0 Collaboration), Phys. Rev. Lett. **100**, 192004 (2008).
375 [8] V. M. Abazov *et al.* (D0 Collaboration), Phys. Rev. D **76**, 072007 (2007); V. M. Abazov *et al.* (D0 Collaboration),
376 Phys. Rev. D **82**, 032002 (2010).
377 [9] V. M. Abazov *et al.* (D0 Collaboration), Phys. Lett. B **626**, 55 (2005).
378 [10] T. Aaltonen *et al.* (CDF Collaboration), Phys. Rev. D **82**, 052002 (2010).
379 [11] G. Aad *et al.* (ATLAS Collaboration), arXiv:1012.1792, submitted to Eur. Phys. J. C.
380 [12] V. Khachatryan *et al.* (CMS Collaboration), Phys. Lett. B **695**, 424 (2011).
381 [13] V. M. Abazov *et al.* (D0 Collaboration), Nucl. Instrum. Methods Phys. Res. A **565**, 463 (2006).
382 [14] T. Andeen *et al.*, FERMILAB-TM-2365 (2007).
383 [15] G. C. Blazey *et al.*, in *Proceedings of the Workshop: "QCD and Weak Boson Physics in Run II,"* edited by U. Baur,
384 R. K. Ellis, and D. Zeppenfeld (Fermilab, Batavia, IL, 2000) p. 47, arXiv:hep-ex/0005012; see Sec. 3.5 for details.
385 [16] V. M. Abazov *et al.* (D0 Collaboration) Nucl. Instrum. Methods Phys. Res. A **620**, 490 (2010).
386 [17] V. M. Abazov *et al.* (D0 Collaboration), Phys. Rev. D **76**, 052006 (2007).
387 [18] M. L. Mangano, M. Moretti, F. Piccinini, R. Pittau, and A. D. Polosa, J. High Energy Phys. **0307**, 001 (2003).
388 [19] T. Sjostrand, S. Mrenna, and P. Z. Skands, J. High Energy Phys. **0605**, 026 (2006).
389 [20] J. Pumplin *et al.* (CTEQ Collaboration), J. High Energy Phys. **07**, 012 (2002).
390 [21] R. Gavin, Y. Li, F. Petriello, and S. Quackenbush, arXiv:1011.3540 [hep-ph].
391 [22] R. K. Ellis, Nucl. Phys. Proc. Suppl. **160**, 170 (2006).
392 [23] S. Frixione and B. R. Webber, arXiv:hep-ph/0612272.
393 [24] A. Buckley, H. Hoeth, H. Lacker, H. Schulz and J. E. von Seggern, Eur. Phys. J. C **65**, 331 (2010);
394 P. Z. Skands and D. Wicke, Eur. Phys. J. C **52**, 133 (2007).
395 [25] P. M. Nadolsky *et al.*, Phys. Rev. D **78**, 013004 (2008).
396 [26] Y. Peters, K. Hamacher and D. Wicke, FERMILAB-TM-2425-E.
397 [27] P. Sinervo, In the *Proceedings of PHYSTAT2003: Statistical Problems in Particle Physics, Astrophysics, and Cosmology,*
398 *Menlo Park, California, 8-11 Sep 2003, pp TUAT004.*
399 [28] The pseudorapidity is defined as $\eta = -\ln[\tan(\theta/2)]$, where θ is the polar angle with respect to the proton beam.